Journal of Membrane Science 551 (2018) 113–122

Contents lists available at ScienceDirect

Journal of Membrane Science

journal homepage: www.elsevier.com/locate/memsci

Cause and effects of hyperskin features on carbon molecular sieve (CMS) membranes

Oishi Sanyal[a], Stephanie T. Hicks[a], Nitesh Bhuwania[b], Samuel Hays[a], Manjeshwar G. Kamath[a], Shweta Karwa[c], Raja Swaidan[d], William J. Koros[a,*]

[a] School of Chemical and Biomolecular Engineering, Georgia Tech, Atlanta, GA, USA
[b] Chevron Corporation, Richmond, CA, USA
[c] Shell International Exploration and Production Inc, Houston, TX, USA
[d] Air Liquide, Delaware Research and Technology Center, Newark, DE, USA

ARTICLE INFO

Keywords:
Carbon molecular sieves
Hollow fiber membranes
Selective skin asymmetry

ABSTRACT

This article considers a previously overlooked feature in carbon molecular sieve (CMS) membranes that we term a "hyperskin" present at the outermost region of dense CMS selective layers. Such a feature with much lower permeability, but similar selectivity compared to the bulk of the skin, reduces CMS hollow fiber permeance below that predicted from corresponding dense films. Effects of the hyperskin are considered for CMS hollow fibers with low skin thicknesses based on two polyimide precursors – Matrimid® and 6FDA:BPDA-DAM. Although the fundamental formation mechanism for the hyperskin feature suggests its existence on virtually all CMS membranes, its impact on transport properties is shown to differ dramatically, depending on the detailed characteristic properties of the specific CMS membrane. Indeed, for hollow fibers with very low nominal resistance (i.e. $\frac{\text{Selective layer thickness determined by SEM}}{\text{Intrinsic permeability of thick dense CMS films}}$), the observed permeance only reaches a *small fraction* of the predicted permeance. The selectivity between different gas penetrants, however, is not altered by the presence of this hyperskin. While identifying this issue is the major focus of this article, strategies to address this limitation, without compromising the molecular sieving properties of CMS membranes are briefly discussed.

1. Introduction

Carbon molecular sieve (CMS) membranes constitute a special class of rigid molecular sieving materials that are easily processable into hollow fiber configurations and exceed polymer performance upper-bound for challenging gas-pairs [1–3]. The formation of defect-free CMS hollow fiber membranes has been established [4]; however, formation of CMS hollow fibers with thin selective layers is an ongoing topic of great importance. Bhuwania et al., reported a silica sol-gel based technique to create thin-skinned CMS fibers for Matrimid® derived CMS [5,6], and in this work we further extend it to 6FDA:BPDA-DAM CMS (henceforth referred to as 6F). The current paper uses CMS membranes derived from these two precursors to show the impact of a new feature, entitled "hyperskin". As explained below, such a feature can have different effects on the performance of different CMS types, depending upon the intrinsic permeability and the selective layer thickness of the specific CMS type.

The chemical structures of the two types of polymeric precursors are shown in Fig. 1.

During pyrolysis, asymmetric polymeric hollow fiber precursors are heated beyond their glass-transition temperatures (T_g) to form their corresponding CMS membranes. Upon passage across the T_g, the porous support substructure collapses tending to cause massive loss in asymmetry. Bhuwania et al., developed a method for suppressing this collapse by treating the polymer precursors with vinyltrimethoxysilane (VTMS), the detailed mechanism of which has been described elsewhere [5,6]. In our earlier work, the technique was shown to increase Matrimid® CMS permeance by ~ 9× by using pure VTMS. In this article we also show efficacy with very dilute VTMS in hexane solutions for Matrimid® precursors. Use of lower concentrations of VTMS facilitates incorporation directly into existing fiber spinning processes, as part of a final solvent exchange step, described later. This technique was extended further to 6F derived CMS which is intrinsically ~ 7× more permeable than Matrimid® CMS when formed by pyrolysis at 550 °C under inert atmosphere (UHP Argon)[7].

For 6F CMS, the skin layer was reduced by ~ 8×, however, the permeance enhancement was only ~ 1.5×, thereby alerting us to an additional resistance. We term this resistance a "hyperskin" present

* Corresponding author.
E-mail address: wjk@chbe.gatech.edu (W.J. Koros).

https://doi.org/10.1016/j.memsci.2018.01.021
Received 11 December 2017; Received in revised form 5 January 2018; Accepted 10 January 2018
Available online 12 January 2018
0376-7388/

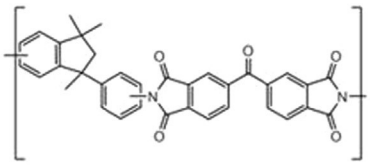

Matrimid® (BTDA-DAPI)

BTDA: 3, 3'-4, 4'-benzophenone tetracarboxylic dianhydride
DAPI: 5(6)-amino-1-(4'-aminophenyl)-1, 3-trimethylindane

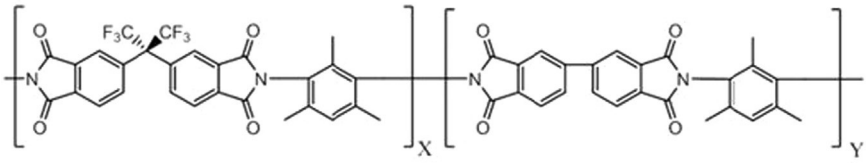

6FDA: BPDA-DAM (X=1; Y =1)

6FDA: 4, 4' (hexafluoroisopropylidene) diphthalic anhydride
BPDA: 3, 3'-4, 4'-biphenyl tetracarboxylic dianhydride
DAM: 2, 4, 6-trimethyl-1, 3-phenylene diamine

Fig. 1. Chemical structures of the repeat units of Matrimid® and 6FDA: BPDA-DAM.

atop the apparent selective layer with lower intrinsic permeability from the bulk selective CMS permeability. Based on additional results presented in this work, it appears that such a hyperskin exists in all types of CMS membranes including dense films; however, its effect is most apparent in V-treated 6F CMS. In this article, we present a fundamental framework to explain the formation and effects of such a feature on CMS with varying morphological characteristics.

2. Theory and background

2.1. Structure of CMS

Controlled high temperature pyrolysis of polyimide precursors is believed to form CMS comprising disordered turbostratic structures, as shown in Fig. 2, with aromatized strands arranged to form plates. Voids between the plates are called micropores, while the slits between the strands are called ultramicropores. The micropores (7–20 Å) act as sorption sites and provide long diffusion jump lengths, thereby providing high intrinsic permeabilities. The ultramicropores (< 7 Å), on the other hand, primarily regulate the sieving properties of the membrane [3].

2.2. Transport in CMS membranes

The intrinsic performance of CMS membranes, like other molecularly selective membranes, is determined by permeability and selectivity factors. Transport through CMS membranes follows the sorption-diffusion mechanism wherein gas molecules first sorb on the upstream side of the membrane. By virtue of the difference in chemical potential, the penetrants are transported to the downstream of the membrane from which they ultimately desorb. The permeability coefficient (or more commonly Permeability), P_A of component A is defined by Eq. (1).

$$P_A = \frac{N_A . l}{\Delta p_A} \tag{1}$$

where N_A is the steady-state flux of penetrant A through a membrane of thickness l caused by a transmembrane partial pressure difference Δp_A. Permeability is also equal to the product of diffusion coefficient (D_A) and sorption coefficient ($\mathbb{S}_A$), shown by Eq. (2)

$$P_A = D_A \times \mathbb{S}_A \tag{2}$$

The pure component sorption coefficient, $\mathbb{S}_A$ equals the sorbed penetrant concentration of A, normalized by the local equilibrium pressure. Sorption in CMS typically follows the Langmuir isotherm model, as shown by Eq. (3).

$$\mathbb{S}_A = \frac{C_A}{p_A} = \frac{C'_{HA} b_A}{1 + b_A p_A} \tag{3}$$

where C_A is the equilibrium uptake of gas A under equilibrium pressure

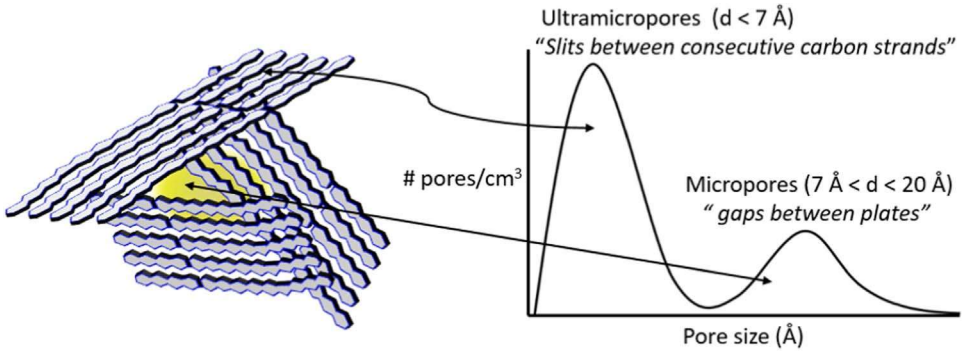

Fig. 2. Turbostratic carbon structure with its idealized micropore and ultramicropore structure. Reproduced with permission from [3].

p_A, and C'_{HA} and b_A are Langmuir capacity and Langmuir affinity parameters respectively.

Permeability is most commonly expressed in Barrers, where

$$1\text{Barrer} = 10^{-10}\frac{\text{cc(STP).cm}}{\text{cm}^2\text{.s. cm Hg}} \quad (4)$$

For non-ideal mixed gas, Δp_A is replaced by the transmembrane fugacity difference.

For asymmetric hollow fibers, due to the uncertainty involved in determining the exact separation layer thickness, the membrane productivity for a penetrant A is usually expressed in terms of permeance $(P/l)_A$, as shown in Eq. (5).

$$\left(\frac{P}{l}\right)_A = \frac{N_A}{\Delta p_A} \quad (5)$$

Permeance is expressed in terms of Gas Permeation Unit (GPU) where

$$1\text{GPU} = 10^{-6}\frac{\text{cc(STP)}}{\text{cm}^2\text{.s. cm Hg}} \quad (6)$$

The ideal selectivity $\alpha_{A/B}$ for two penetrants, A & B, is represented by Eq. (7) as the ratio of the pure component permeabilities or permeances.

$$\alpha_{A/B} = \frac{P_A}{P_B} = \frac{(P/l)_A}{(P/l)_B} \quad (7)$$

3. Materials and methods

3.1. Materials

Two types of polymer precursors were used: Matrimid® and 6FDA:BPDA-DAM [1:1]. The structures of both precursor materials are shown in Fig. 1. Matrimid® was purchased from Huntsman International LLC (Salt Lake City, UT) and 6FDA: BPDA-DAM from Akron Polymer Systems (Akron, OH). *Sure-seal* bottles of vinyltrimethoxysilane (VTMS) (97% purity), hexane, 1-methyl-2-pyrrolidine (NMP), ethanol, tetrahydrofuran (THF) and acetone were purchased from Sigma-Aldrich (St Louis, MO). For the solvent exchange of polymer fibers, methanol (20 L) and hexane (20 L) were purchased from BDH Chemicals Co. Pure-component CO_2 and CH_4 gases (Research Grade Quality) were purchased from Airgas (Radnor Township, PA), while 50:50 CO_2:CH_4 mixed gas (± 1% blend accuracy) was purchased from Nexair (Memphis, TN). All fittings used for module making were purchased from Swagelok® Georgia.

3.2. Asymmetric hollow fiber spinning

Asymmetric Matrimid® hollow fibers were spun using a conventional dry-jet/wet-quench method [8]. In short, the polymer dope (consisting of dried polymer powder, solvents and non-solvents) was co-extruded with a bore solution (consisting of an optimized solvent and non-solvent mixture) through a spinneret and quenched in water-bath. Between the spinneret and the quench bath, an air-gap was maintained to facilitate evaporation of the volatile solvent and enable formation of a dense selective layer. The phase separation induced by the water quench forms the porous substructure (transition layer + macroporous support). The fibers were collected on a rotating drum, followed by solvent exchange with methanol and hexane. Finally the fibers were dried under vacuum at 75 °C for 2 h. The dope and bore fluid compositions along with the spinning conditions for the Matrimid® precursor used for this work are shown in Table 1.

The 6F precursors were supplied by Air Liquide (Newark, DE). The dope composition and the spinning details for these precursors are confidential, however the composition and spinning details are similar to those described previously [9,10] and also noted above for Matrimid®.

Table 1
Detailed spinning parameters and conditions for Matrimid® hollow fiber precursor spinning.

Matrimid® dope composition	
Component	**wt%**
Matrimid® powder*	26.2
NMP	53.0
Ethanol	14.9
THF	5.9
Bore-fluid composition	
Component	**wt%**
NMP	90.0
DI Water	10.0
Spinning conditions	
Parameters	**Conditions used****
Dope flow rate	180 ml/h
Bore flow rate	60 ml/h
Dope temperature	60 °C
Dope line temperature	60 °C
Spinneret temperature	60 °C
Quench bath temperature	50 °C
Air-gap	15 cm
Drum take-up rate	15 rpm

* The polymer powder was dried overnight in a vacuum oven at 150 °C.
** The dope was heated up to the required temperature and allowed to degas overnight in order to avoid bubble formation while spinning. All other components of the spinning setup were also allowed to equilibrate at their desired temperatures overnight.

3.3. Vinyltrimethoxysilane (VTMS) treatment of precursor fibers (V-treatment)

For cases involving V-treatment, the precursor fibers were soaked in VTMS solutions of selected concentrations in hexane for 24 h. Following the soaking period, excess VTMS solution was removed by light blotting with Kimwipes®. The fibers were then transferred to a glove-bag which was maintained at 100% RH by flowing compressed air through DI water. The glove-bag was inflated and deflated four times before being sealed to ensure 100% RH, and the fibers were stored in it for another 24 h. Upon exposure to moisture, VTMS crosslinks on the support "struts" comprising the porous substructure of the precursor fibers via a standard sol-gel crosslinking reaction [11]. Following this moisture-induced crosslinking step, the fibers were dried in vacuum overnight at 150 °C to remove residual VTMS and moisture. The V-treated fibers were then pyrolyzed at 550 °C/UHP Argon to form CMS hollow fibers using the protocol described in Table 2 in the following section.

3.4. Formation of CMS hollow fibers from polymer hollow fibers

Pyrolysis was performed in a three-zone furnace (model # XST-3-024-3C, Thermcraft, Inc., Winston-Salem, NC) with controller to achieve a uniform pyrolysis zone (Model # CN1507TC, Omega Engineering Inc. Stanford, CT). The schematic of the pyrolysis setup is shown below in Fig. 3. The fibers were placed on a stainless steel wire mesh (McMaster Carr, Robbinsville, NJ) and loaded into a quartz Tube

Table 2
Standard 550 °C/UHP Argon pyrolysis protocol.

$T_{initial}$ (°C)	T_{final} (°C)	Ramp rate (°C/min)
50	250	13.3
250	535	3.85
535	550	0.25
550	550	2 h soak

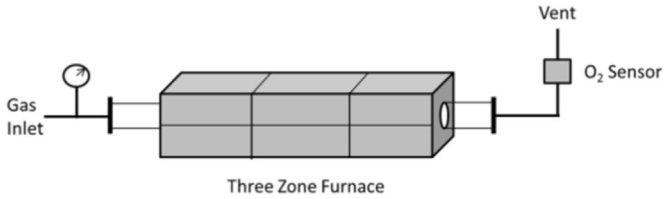

Fig. 3. Schematic of three-zone furnace used for pyrolysis.

(55 mm ID and 4 ft. long) (National Scientific Co. Quakertown, PA). The ends of the tube were sealed with metal flanges and Silicon O-rings (Model # EQ-FI-60, MTI Corporation, Richmond, CA). For all experiments described in this paper, the pyrolysis was carried out under an inert atmosphere by maintaining a constant flow of 200 cc (STP)/min UHP Argon (Airgas). Flow rate of the purge gas was monitored by a mass flow controller (model # MC-500-SCCM-D, Alicat Scientific, Marana, AZ).

Purging was done for at least 8 h, and the O_2 concentration was monitored by an oxygen analyzer (Rapidox 2100 Series, Cambridge Sensotec Ltd, Cambridge, England). A thorough procedure was used for cleaning the parts of a furnace between each consecutive run for V-treated CMS and after 4–5 runs for untreated CMS. The 1/8″ SS tailpipe, which was connected to the output of the O_2-sensor on one end and the vent on the other end was replaced, whenever the rest of the parts were cleaned. The cleaning protocol is outlined below:-

1. All parts were soaked in hot NMP (T ~ 100 °C) for ~ 8–12 h
2. Next, parts were soaked in acetone for ~ 4–6 h
3. Finally the parts were dried in a convection oven (T ~ 110 °C) for ~ 30 min before reassembly.

The quartz tube and the mesh were rinsed with acetone and baked under 500 cc (STP) air/ min at 900 °C for ~ 6–8 h to remove any undesirable residues having the potential of affecting subsequent pyrolysis runs. After ≥ 8 h of UHP Argon purging and ensuring that the O_2 sensor value ≤ 1 ppm, the fibers were pyrolyzed using the profile below

Following the soak period, the furnace was allowed to naturally cool to 50 °C under constant UHP Argon purge before the CMS fibers were removed.

3.5. Hollow fiber permeation tests

3.5.1. Construction of hollow fiber modules

The fibers were potted in lab-scale modules, the details of which can be found elsewhere [12] using 3M DP-100 epoxy. For *polymer* precursors, 6 fibers were potted in each module of effective length of ~ 20–30 cm. For the higher permeance *CMS fibers*, only one fiber was potted in each module of ~ 11–12 cm effective length. The precursor fibers were tested in constant pressure permeation systems and the CMS fibers were tested ~ 24 h after being potted in modules in constant volume systems.

3.5.2. Constant volume permeation

The CMS hollow fiber modules were tested in constant volume permeation systems at 35 °C, the details of which can be found in [13]. Prior to starting the permeation, the upstream and downstream sides were evacuated for ~ 30 min, making sure the leak rate was ≤ 1% of the gas permeation rate. For all experiments described below, mixed gas tests were performed with 50:50 CO_2:CH_4. Unless otherwise mentioned, the upstream pressure was maintained at 100 psia and 1% stage cut was maintained during the experiments to avoid effects of concentration polarization. The mixed-gas was fed to the shell-side of the module and the bore-side permeate flow rate was measured by recording the pressure rise in a known downstream volume. Both the upstream and downstream pressures were monitored by pressure transducers. The composition of the permeate was analyzed using a gas chromatograph (Bruker 450) equipped with a Thermal Conductivity Detector (TCD). Replicates were tested for all conditions described in the subsequent sections to ensure data reproducibility.

3.6. Imaging using scanning electron microscopy (SEM)

Zeiss Ultra60 Fe-SEM was used for characterizing polymer precursor and CMS morphologies. Polymer precursor samples were prepared by immersion in hexane followed by fracturing in Liquid Nitrogen. CMS samples were prepared by simply fracturing them by hand. All samples were put on a carbon tape and attached on suitable SEM stubs. The polymer samples were sputter coated with gold using Hummer 6 Gold/ Palladium Sputterer for 5 min to avoid "sample charging". CMS samples did not require any sputter coating.

4. Results and discussion

4.1. Substructure collapse in CMS hollow fibers

As noted earlier, support substructure collapse occurs during the pyrolysis process after the temperature exceeds the glass transition temperature (T_g) of the precursor material [4–6]. Densification of the transition and macroporous layers occur as the polyimides pass their respective T_g's, reflected by a drastic loss in storage moduli [5]. Since Matrimid® has a lower glass transition temperature (T_g) than 6FDA:BPDA-DAM (305 °C vs 424 °C), a higher degree of collapse is seen in the Matrimid® derived CMS. The following SEM images (Fig. 4) show the precursor and the corresponding CMS formed by 550 °C/UHP Argon pyrolysis for both Matrimid® and 6F.

In the precursor stage, both polyimide fibers show < 1 μm dense selective layers, mesoporous transition layers which are not easily discernible and macroporous supports. Such asymmetric structures are highly desirable in ensuring high membrane productivities; however CMS hollow fibers formed from these polyimide precursors do not retain initial asymmetry. Based on SEM images, the selective skin layer of Matrimid® CMS was ~ 40 μm thick, while that of 6F CMS was ~ 26 μm. The Matrimid® CMS shows a completely densified structure with no porous substructure, while for 6F CMS, the selective skin thickness roughly amounts to ~ 50% of the wall thickness, thereby retaining some of its asymmetry. This phenomenon is clearly not desirable since despite intrinsically high CMS permeabilities in dense film configurations, they cannot be translated into *high-productivity hollow fibers*.

The precursors, used in both cases were defect-free and the CMS formed from them were consequently defect-free as well. The transport properties of the precursors used (shown in Fig. 4A&B) are included in the Supplementary material (Table S4). Based on the dense film permeabilities and the selective layer thickness evident from SEM (L_{SEM}), the expected P/L of the CMS hollow fibers can be theoretically estimated. As shown in Table 3, the estimated P/L was in agreement with the experimental P/L for *both types* of CMS membranes.

4.2. Restricting sub-structure collapse by V-treatment

Restriction of sub-structure collapse was enabled by the so-called V-treatment referred to earlier, which is a silica sol-gel based technique. The mechanism and details of this process have been described elsewhere [5,6]. In short, after the precursor fibers are saturated with VTMS, the methoxy groups present in VTMS are hydrolyzed in the presence of humidity to undergo condensation and form Si-O-Si cross-links, as shown in Fig. 5a. This cross-linked silica provides reinforcing sheaths on the "struts", thereby providing support to the porous substructure to prevent complete collapse beyond T_g, as depicted schematically in Fig. 5b. The effect of the V-treatment process was essentially limited to the porous substructure and had no significant effect on the properties of the CMS selective skin layer. This was previously

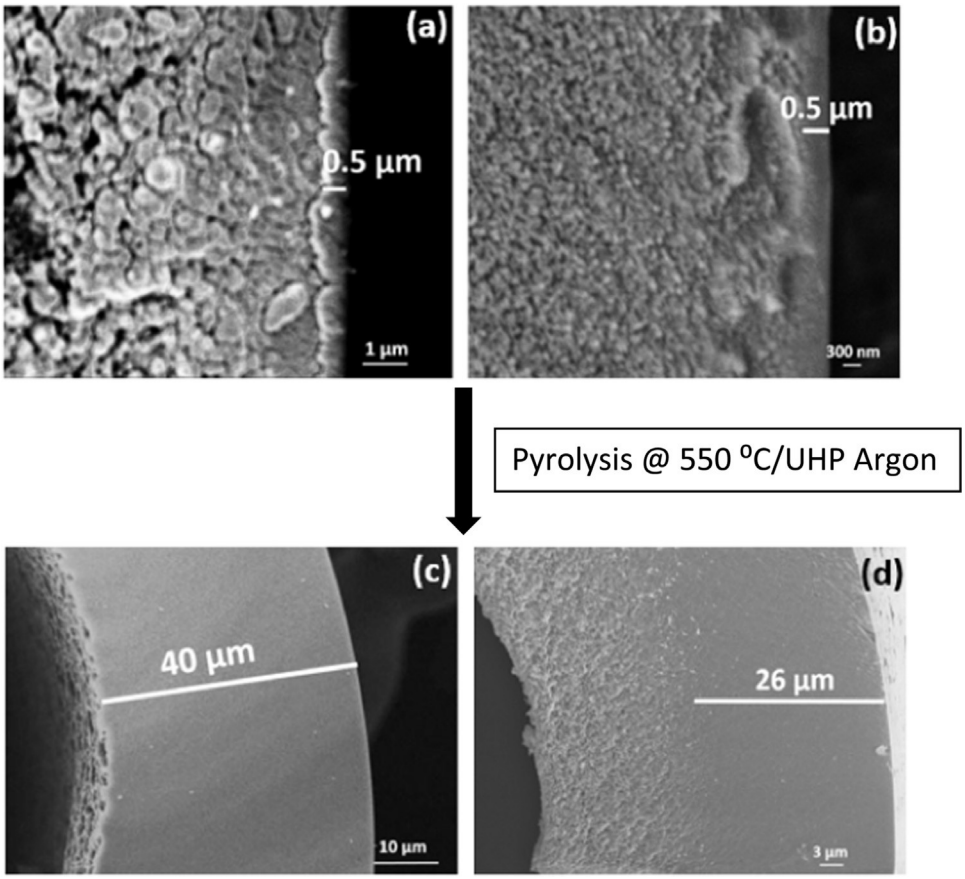

Fig. 4. SEM images of (a) Matrimid® precursor (b) 6FDA:BPDA-DAM precursor (c) Matrimid® CMS 550 °C/UHP Argon [4] and (d) 6FDA:BPDA-DAM CMS 550 °C/UHP Argon.

Table 3
Transport properties of CMS dense films and untreated CMS hollow fiber membranes.

Type	Dense film CO_2 P (Barrer)	L_{SEM} (µm)	Estimated CO_2 P/L (GPU)	Observed CO_2 P/L (GPU)
Matrimid®	1049 ± 100 [7]	~ 40	~ 26	23 ± 1
6F	7170 ± 700 [7]	~ 26	~ 275	260 ± 30.3

shown by X-ray Photoelectron Spectroscopy (XPS) analysis on V-treated Matrimid® CMS by Bhuwania et al. and is likely applicable to V-treated 6F CMS as well [5]. In fact, the effect for 6F is expected to be even less due to the evolution of fluorinated by-products during the pyrolysis of 6F precursors which can etch off silica [6]. Extensive silica analysis was not done as part of this work, but as noted above, in our previous work, detailed XPS characterization was done on Matrimid® CMS [6] and in one of our very recent work, some Energy Dispersive X-ray Spectroscopy (EDS) analyses were shown for V-treated CMS derived from 6FDA-DETDA:DABE precursor [14].

The V-treatment process enables the formation of relatively thin-skinned CMS fibers from both Matrimid® and 6F precursors, as shown in Fig. 6.

Clearly, complete avoidance of substructure collapse was not achieved as evident from the CMS selective layer being considerably thicker than that of the corresponding precursor fibers; however the improvement was definitely significant. For the Matrimid® CMS, ~ 9× reduction in skin thickness was achieved while for 6F CMS, there was a reduction of ~ 8×.

Table 4 shows the transport properties of CMS hollow fibers formed from V-treated Matrimid® and 6F precursors. With the reduction in skin thickness, the resulting asymmetric CMS fibers formed from the two different membrane materials showed improved P/L, as would be expected. The estimated P/L was compared to the experimental P/L, as was done for the untreated CMS hollow fibers.

For Matrimid® CMS, the permeance increased by ~ 9× from 25 GPU → 216 GPU which was essentially proportional to the reduction in skin thickness from 40 µm → 4–5 µm. [We discovered that the P/L obtained for the V-treated CMS was twice as high as the P/L that we had previously reported [5]. A recently observed aspect of the pyrolysis process is the necessity to clean the different parts of the furnace following every run involving V-treated CMS. This was done rigorously in the current work. Failing to do so leaves trace amounts of contaminants which can back-diffuse from tail-pipes and affect the subsequent run. *This cleaning step has only been recently introduced as a part of our pyrolysis protocol and we provide the relevance of this cleaning protocol in the* Supplementary information (Tables S1-S3)].

For the 6F CMS, the thickness of the selective layer was reduced from 25 µm → 3 µm (~ 8×) but the P/L was enhanced only by a factor of ~ 1.5× from 260 GPU → 400 GPU. [Again, this was carefully shown not to be due to contaminants by doing the pyrolysis runs in a carefully cleaned-out furnace. Previously, a 5× improvement was shown for O_2-doped 6F CMS, but some of these earlier results [5] were also affected by furnace contaminants. This separate topic is covered in detail in the Supplementary material]. Furthermore, the expected P/L for V-treated Matrimid® CMS was in very good agreement with its experimental value. *However for the V-treated 6F CMS, the P/L's differed by a factor of 6*. Based on dense film permeabilities and L_{SEM}, the expected P/L of 6 F CMS was ~ (7170 Barrer / 3 µm) = 2400 GPU, while in practice, a P/L ~ 400 GPU was observed.

Two possible reasons were hypothesized to explain the 6× deviation between the $(P/L)_{estimated}$ vs. $(P/L)_{observed}$ for 6F-CMS:

1. Since the untreated CMS did not show such discrepancies, it was possible that the V-treatment process left some additional silica, which gave rise to an additional surface resistance for 6F CMS.

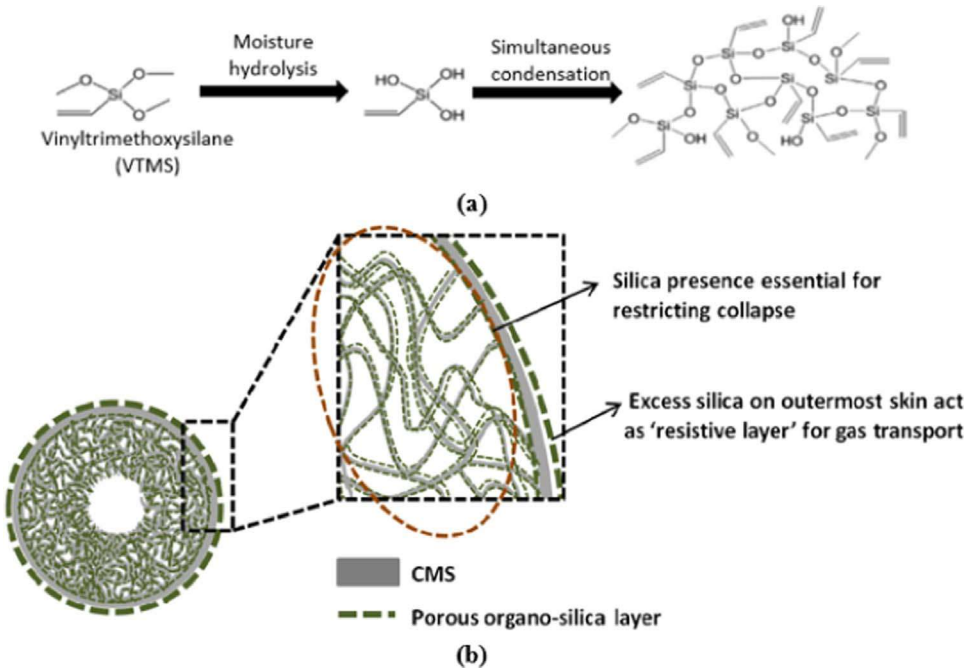

Fig. 5. (a) Mechanism of VTMS crosslinking and (b). Schematic representation of the sub-structure collapse enabled by V-treatment. Reproduced with permission from [5].

2. There was an additional resistance inherent in the carbon that prevented the permeance of the asymmetric 6F CMS from reaching the expected value.

To determine whether either or both factors explain the surprising trends noted above, these issues are considered in the following two Sections (4.2.1 and 4.2.2).

4.2.1. V-treatment effects

4.2.1.1. Effect of VTMS concentration. Additional silica resistance due to VTMS treatment, if present, can be minimized by using lower concentrations of VTMS instead of pure VTMS. This straightforward approach was applied to both Matrimid® and 6F CMS 550 °C/UHP Argon. For Matrimid® CMS, a 9× enhancement in permeance proportional to the 9× reduction in skin thickness was already achieved using pure VTMS; hence as expected, within experimental

Table 4
Transport properties of CMS dense films and V-treated CMS hollow fiber membranes.

Type	Dense film CO_2 P (Barrer)	L_{SEM} (μm)	Estimated CO_2 P/L (GPU)	Observed CO_2 P/L (GPU)
Matrimid®	1049 [7]	~ 5	~ 210	216 ± 23
6F	7170 [7]	~ 3	~ 2400	394 ± 50

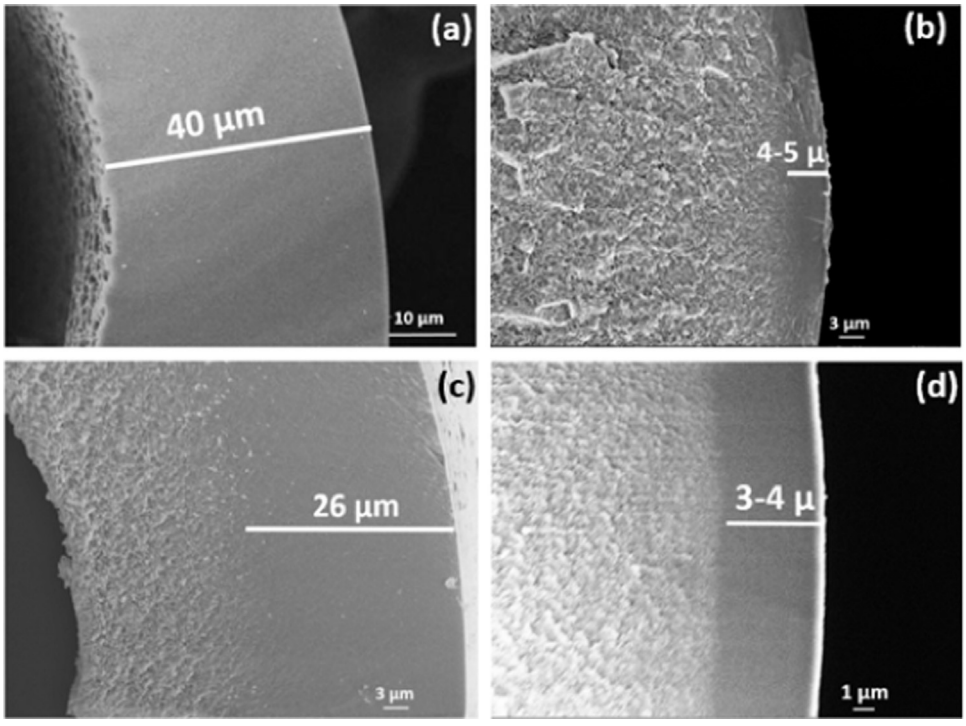

Fig. 6. SEM images of (a) Untreated Matrimid® CMS [4] (b) V-treated Matrimid® CMS (c)Untreated 6F CMS and (d) V-treated 6F CMS.

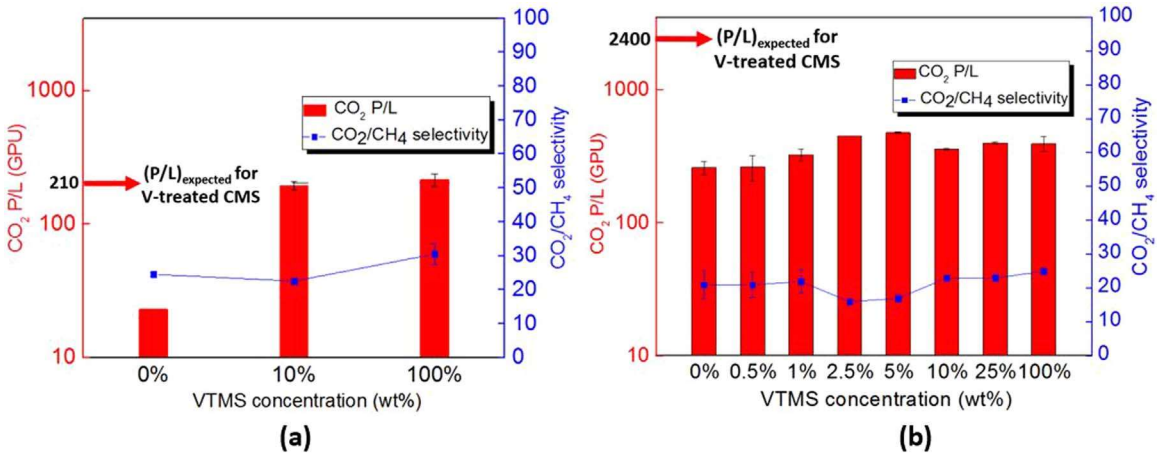

Fig. 7. Effect of VTMS concentration on the transport properties of (a) Matrimid® 550 °C/UHP Argon CMS and (b) 6F 550 °C/UHP Argon CMS.

uncertainty, no further P/L enhancement was seen at lower VTMS concentrations. This fact notwithstanding, using a simple dilute VTMS-hexane solution is appealing to enable easy introduction into the precursor formation process, which as described before, utilizes hexane as one of the solvents during the solvent-exchange step. Since the 6F CMS experiences the large (6×) discrepancy between the expected P/L and the experimentally observed P/L, it was more vital to check the effect of low VTMS concentration for this case. It is significant that in the case of 6F precursor, essentially no benefits are observed in actual results despite the SEM results showing efficacy with all VTMS concentrations. A 10 wt% solution of VTMS dissolved in hexane was found to be sufficient to effectively produce a thin-skinned Matrimid® CMS, without any discernible change in performance or selective skin thickness in comparison to the pure VTMS case. The transport properties of Matrimid® CMS with varying VTMS concentrations are plotted in Fig. 7a.

For 6F CMS, the VTMS concentration required to resist substructure collapse could be further lowered in comparison to Matrimid® CMS, as shown in Fig. 7b. This could be explained by the fact that the degree of sub-structure collapse in 6F CMS was already less than that of Matrimid®. Some performance variations were observed with varying VTMS concentrations but more importantly, even with low concentrations like 2.5 wt%/5 wt%, *the expected P/L ~ 2400 GPU could not be attained*. The CO_2/CH_4 selectivities for the V-treated CMS fibers remain practically equal to that of untreated CMS as well as dense films for both Matrimid® and 6F.

The following SEM images, shown in Fig. 8a & b show the selective layer of Matrimid® and 6F CMS with 10 wt% VTMS concentrations respectively. As noted before, although the P/L was not improved significantly with lower VTMS levels, this pre-pyrolysis step can be incorporated in the spinning process for both Matrimid® and 6F precursors, thereby making the process easily scalable.

4.2.1.2. CMS insensitivity to VTMS concentrations – explanation. The above results show that the performance of both Matrimid® and 6F CMS were *essentially independent* of the VTMS concentration used, within minor experimental uncertainty. In this section, we clarify these results by using a series-resistance model as shown in Eq. (8). In this analysis, we consider whether with higher VTMS concentrations, a non-selective silica layer remains on the CMS surface which potentially adds to the resistance offered to gas permeation. This simple model makes a conventional assumption that the overall resistance (inverse permeance) is a sum of the resistance from the top silica layer and the resistance from the underlying carbon.

$$\frac{L_{total}}{P_{total}} = \frac{L_{Silica}}{P_{Silica}} + \frac{L_{CMS}}{P_{CMS}} \quad (8)$$

In the above expression, L_{Silica} represents any unwanted silica layer remaining on the CMS surface post-pyrolysis with a permeability represented by P_{Silica}, while L_{CMS} represents the selective layer of the underlying CMS membrane with an inherent permeability of P_{CMS}. Although the exact value of P_{Silica} is not known, using a value of ~ 1500 Barrer, as reported by Adams et al. [15] for heat-treated silica is reasonable. We further consider a hypothetical case, where both V-treated Matrimid® and 6F CMS have equal values for L_{Silica}. In the case of V-treated Matrimid® CMS, P_{CMS} ~ 1050 Barrer and L_{CMS} ~ 5 μm, while for 6F-CMS, P_{CMS} ~ 7170 Barrer and L_{CMS} ~ 3 μm [**Note**: $L_{CMS} = L_{SEM} - L_{Silica}$; since L_{Silica} is likely very small, for convenience sake, L_{CMS} is taken to be equivalent to L_{SEM}] Hence for V-treated Matrimid®, the $(\frac{L_{CMS}}{P_{CMS}})$term, i.e. the resistance from bulk CMS ~ 4.7×10^{-3} [μm Barrer^{-1}], while for V-treated 6 F, it is ~ 4.2×10^{-4} [μm Barrer^{-1}]. In the case of Matrimid® 550 °C/UHP Argon CMS, since

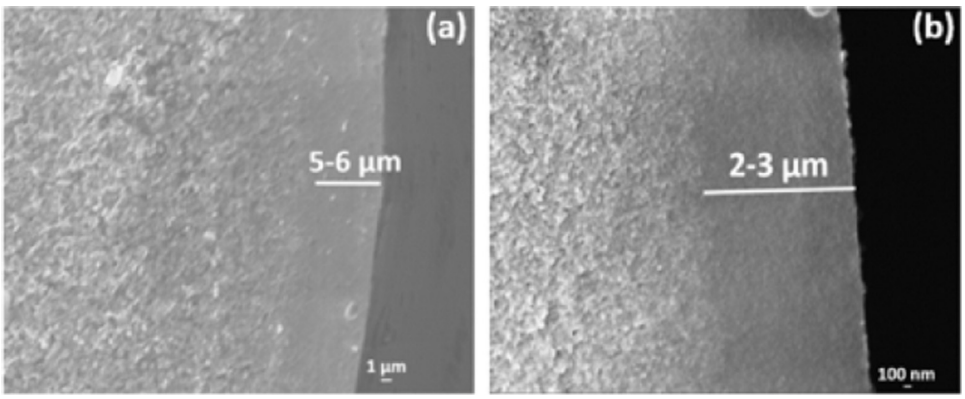

Fig. 8. SEM images showing the selective layer of (a) 10% V-treated Matrimid® 550 °C/UHP Argon CMS and (b) 10% V-treated 6F 550 °C/UHP Argon CMS.

$P_{Silica} \sim P_{CMS}$ and L_{Silica} is insignificant, the effect of any small silica resistance, if at all present at higher VTMS concentrations, *does not affect the final performance beyond experimental uncertainty*.

For 6F 550 °C/UHP Ar CMS, the CMS resistance term is roughly *an order of magnitude lower* than that of Matrimid® but $P_{Silica} \sim \frac{1}{7}P_{6F\,CMS}$. Clearly therefore, in theory, if silica is an important factor, the transport properties of V-treated 6F CMS should be severely affected by the presence of excess silica as the concentration of VTMS solution is increased. However, the experimental observations *did not* show this pattern. As hypothesized by Bhuwania, the evolution of CHF_3 and HF during the pyrolysis of 6F precursor can etch away a considerable portion of silica, virtually eliminating the additional surface silica layer resistance [6]. Since Matrimid® lacks fluorinated groups, the silica etching effect is absent in its case; however, in both cases, *effects of residual silica are negligible*. This fact notwithstanding, this analysis shows that asymmetric CMS membranes formed from *non-fluorinated polymeric precursors* such as Matrimid® could also be affected if the selective layer can be sufficiently thin. For such non-fluorinated precursors reducing the VTMS concentration is a powerful tool for optimizing observed P/L of the final CMS fiber.

In any case, the current analysis shows that the role of silica in lowering the P/L of V-treated 6F CMS below the expected value is negligible. This fact indicates that the presence of an additional resistance inherent in such carbon membranes appears to be the likely cause of discrepancy in measured *vs.* calculated P/L which was noted above for the 6F precursors. This observation leads to the discussion of a potential "hyperskin" atop the overall selective layer which can contribute to the lower permeance of 6F CMS compared to its estimated value. The following sections are entirely dedicated to this topic.

4.2.2. Additional previously unrecognized transport resistance

4.2.2.1. The concept of a hyperskin. A recent study by Liao et al. [16] using Positron Annihilation Lifetime Spectrometry (PALS) for Kapton® 900 °C/UHP Ar CMS showed the presence of surprising asymmetry within a normally *dense CMS film*. Such a layer is analogous to the dense selective layer in asymmetric fibers. In Fig. 9 adapted from the article, the S parameter (plotted along the Y-axis) indicates the variation of pore volume as a function of film depth. This study clearly shows the presence of a "porosity gradient" in the *normally dense layer* wherein portions of the film differ in porosity from the "bulk CMS". As the soak time was increased from 2 to 4 h, the portion of the film with the lowest S parameter was extended through a larger film depth. For convenience, we refer to this portion as the "hyperskin" and owing to its low porosity, this hyperskin is envisioned to have lower permeability as well, compared to the remaining bulk of the skin. It should be noted here, that with longer soak, the porosity of the "bulk CMS" which

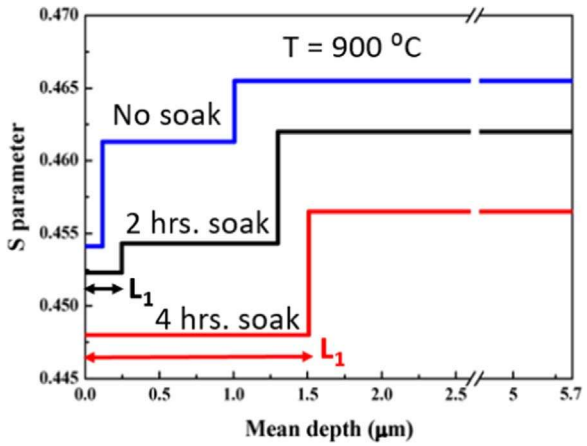

Fig. 9. Evidence of "selective skin asymmetry" in Kapton® CMS dense film shown with PALS technique. Reproduced with slight modifications with permission from [16].

essentially is still the major portion of the dense film, also decreases progressively. This has been observed by Steel et al. [17] that longer soak times lead to a loss in permeability due to tightening of the micropores between the ultramicroporous plates (as shown in Fig. 2) comprising the selective CMS.

Based on the PALS study, the "asymmetric" skin essentially comprises two or more regimes with differing permeabilities. To analyze the formation and more importantly, to understand the effects of the hyperskin on the transport properties of the CMS membranes, a simplified picture consisting of just two well-defined porous regimes (hyperskin and bulk CMS) can be used, as shown in Fig. 10a.

To understand the formation of the hyperskin the pyrolysis process must be revisited. During the thermal ramping step of pyrolysis, the polyimide chains are fragmented into rigid aromatized strands which organize to form ultramicroporous carbon plates during the soak period at the final 550 °C [17]. In this stage, the plates can be visualized to organize in a way as shown in Fig. 10b (left). We hypothesize that during the 2 h soak time at 550 °C while the carbon plates are organizing and settling, the top few surface layers at the gas-CMS interface, which have higher mobility, undergo a rapid *thin film aging* process [18,19]. Specifically, for plates at this interface, edge contacts with neighboring plates is lacking, and a more or less- "house of cards" collapse is envisioned to occur starting at this interface and progressing inward. These top few layers comprising effectively stacked plates with collapsed inter-plate distances, are represented by L_1 in Fig. 10a & b (right). On the other hand, the remaining bulk of the skin with its inherent microporous structure is represented as L_2. Such large scale rearrangement with plates cause major reduction in permeability by reducing both sorption and diffusion coefficients. Such rearrangements, however, *do not change diffusion selectivity*, which is determined primarily by the distribution of ultramicropores *between the carbon strands* in respective plates. Moreover, sorption selectivity, which is primarily determined by condensability differences between penetrants (e.g., CO_2 *vs.* CH_4) will not be dramatically affected either. Hence the overall *permselectivity remains unaltered*.

Clearly, formation of such a dense hyperskin is undesirable for productivity, and factors such as the final pyrolysis temperature, high temperature exposure periods involving both soak times and cooling rates, are envisioned to influence its properties. This process occurs in parallel with the micropore and ultramicropore perfection processes which are desirable to impart attractive separation properties to the membranes. The effect of this hyperskin on the transport behavior of different CMS membranes can be elucidated with a "series resistance" argument, as elaborated in detail in the following section.

4.2.2.2. Understanding effects of hyperskin on CMS transport properties. Clearly, the hyperskin, even though presumably present in all CMS membranes, does not affect the transport properties of all membranes equally. As discussed before, among the 4 types of hollow fiber CMS membranes – untreated and V-treated Matrimid® and untreated and V-treated 6F, the hyperskin effect is only strongly felt by the V-treated 6F CMS. This can be once again explained by the series resistance model. As shown in Fig. 10a, neglecting any negligible silica effects based on Section 4.2.1, the selective skin comprises the hyperskin (L_1) and the bulk CMS (L_2). Hence the total resistance (inverse P/L) is the sum of the resistances from L_1 and L_2, as the following model (Eq. (9)) shows.

$$\frac{L_{total}}{P_{total}} = \frac{L_1}{P_1} + \frac{L_2}{P_2} \tag{9}$$

P_1 and P_2 are the respective permeabilities of L_1 and L_2 regions of Fig. 10 respectively. The P_2 is essentially the intrinsic CMS permeability as discussed below. Based on this model, the overall resistance ($\frac{L_{total}}{P_{total}}$) will significantly deviate from the intrinsic CMS resistance ($\frac{L_2}{P_2}$) if the hyperskin resistance ($\frac{L_1}{P_1}$) becomes large. In other words, the hyperskin

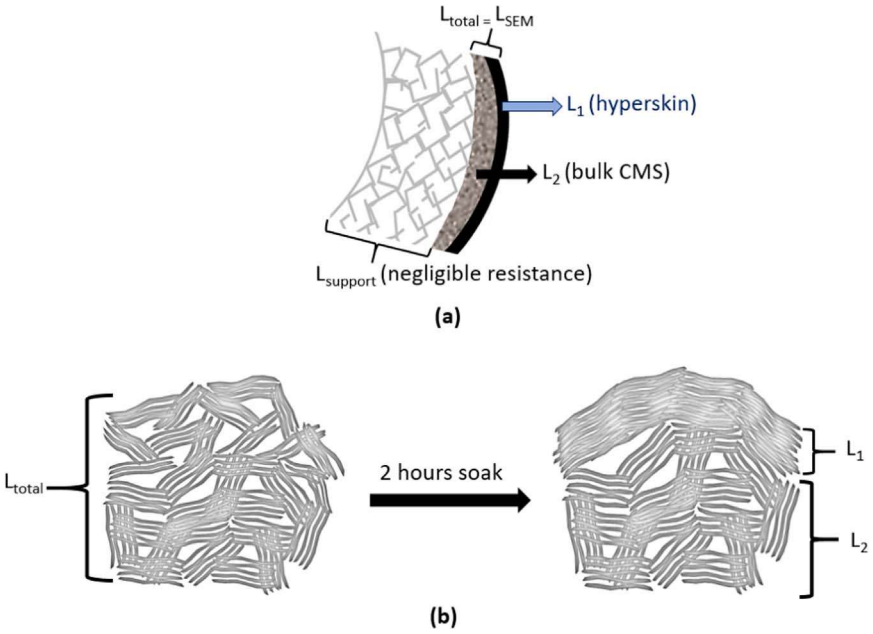

Fig. 10. (a) The presence of a hyperskin atop the selective layer of CMS hollow fibers and (b) the envisioned formation process of a hyperskin during the pyrolysis process.

Table 5
The bulk CMS properties of the 4 CMS types.

CMS type	L_2 (μm)	P_2 (Barrer)	Intrinsic resistance (L_2/P_2) (μm/Barrer)
Untreated Matrimid® CMS	40	1050	3.8×10^{-2}
V-treated Matrimid® CMS	5	1050	4.8×10^{-3}
Untreated 6F-CMS	26	7170	3.6×10^{-3}
V-treated 6F-CMS	3	7170	4.2×10^{-4}

resistance can potentially become the dominant resistance if the inherent CMS resistance becomes too small. The latter depends on the properties (L_2, P_2) of the different CMS fibers. The situations under which this resistance can potentially become very small are: (i) low L_2 (i.e. low selective skin thickness), (ii) very high P_2 (i.e. high intrinsic permeability) and (iii) a combination of both low L_2 and high P_2. To facilitate an easier analysis of the hyperskin effect on each individual membrane, the intrinsic properties of the 4 types of CMS membranes discussed above are tabulated in Table 5.

Assumption: Ideally, $L_2 = L_{SEM} - L_1$, but according to the PALS study since L_1 is very small, $\mathbf{L_2 \sim L_{SEM}}$.

It is evident that the untreated Matrimid® CMS had the highest intrinsic resistance by virtue of having both a large skin thickness and a low permeability. Therefore, the hyperskin resistance has virtually no effect on its transport properties and hence no deviation was observed between its estimated P/L and experimentally observed P/L. With the same P_2, the V-treated Matrimid® CMS had an order of magnitude lower resistance than its untreated counterpart because of lower skin thickness. While the effect of hyperskin is relatively more dominant in this case, its effect is still not evident from the transport properties of this particular CMS. Similarly, the untreated 6F-CMS was able to circumvent the hyperskin resistance by virtue of having a high L_2 value, in spite of having $\sim 7\times$ P_2 than Matrimid® CMS. Finally, the V-treated 6F CMS had $\sim$ *an order of magnitude* lower resistance than untreated 6F/ V-treated Matrimid® CMS and $\sim$ *2 orders of magnitude* lower resistance than untreated Matrimid® CMS. This causes the hyperskin resistance to be the dominant resistance within the selective layer and leads to the $6\times$ discrepancy between the estimated and experimental P/L. Hence, the extent of the hyperskin effect is a strong function of the characteristic properties of the CMS hollow fiber. As shown by the PALS study, even dense CMS membranes have hyperskins but these films are usually $\geq$ 50 μm thick and hence the transport properties practically remain unaltered. This analysis further shows that this issue of selective skin asymmetry can affect all CMS membranes with low inherent resistance. In fact, this was also observed for CMS derived from the precursor, 6FDA-DETDA: DABE wherein the observed CO_2 P/L (450 GPU) of the asymmetric CMS was only $\sim$ 4% of the expected CO_2 P/L of 12000 GPU (12,000 Barrer/1 μm)[14]. Ways to suppress the formation of hyperskin or minimize its effect are clearly directions for future research, and are underway.

5. Conclusions and future work

In this paper, a VTMS-based sol-gel technique developed previously to restrict substructure collapse in asymmetric CMS hollow fibers, was applied on both Matrimid® and 6F 550 °C/UHP Ar CMS. While the method enabled both the CMS membranes to attain higher P/L, significant property differences were noted for the two CMS materials. For the comparatively low permeability Matrimid® CMS, the VTMS technique enabled a $9\times$ reduction in skin thickness, while simultaneously enhancing the P/L by the same factor, relative to non V-treated CMS. However, the P/L for the V-treated 6F CMS only increased $\sim 1.5\times$ relative to the untreated 6F-CMS, in spite of $8\times$ reduction in apparent skin thickness. To explain this, the concept of a hyperskin was introduced in this paper. This feature comprises a submicron skin within the selective layer with highly reduced inter-micropore distances leading to reduced hyperskin permeability. A recent study showing the asymmetry within dense CMS films using PALS as the characterization technique supports the proposed hyperskin concept. It would be definitely worthwhile to do the PALS analysis on asymmetric CMS fibers pyrolyzed from Matrimid® and 6FDA:BPDA-DAM precursors. We do not currently have the ability to perform such PALS analysis, and hope to collaborate with a group that has this capability as part of our ongoing efforts to address and eliminate the hyperskin effects in CMS membranes.

We believe, such hyperskins form in CMS membranes during high temperature exposure periods. On this basis, the final temperature, the soak period and even the cooling rates are consequential to hyperskin formation and the extent of its effect on the transport behavior. We believe hyperskins exist in all the 4 types of CMS – Matrimid®, 6F and their V-treated counterparts, but we showed as to why only in the case

of the V-treated 6F CMS, its presence exerts a strong influence on the overall P/L of the membrane. Our future work will focus on mitigating this effect to allow the asymmetric CMS hollow fiber membranes effectively attain high productivity levels as predicted from dense CMS films. Based on our analysis of the 4 different CMS types, it should be reasonable to conclude that all asymmetric CMS hollow fibers with thin selective layers and high intrinsic permeabilities will encounter this effects such as discussed herein. Overcoming this limitation will naturally place CMS membranes in an even more competitive position in terms of commercial applicability.

Acknowledgments

The authors thank the Office of Basic Energy Science of the U.S. Department of Energy (DE-FG02-04ER15510) for financial support of this work.

Appendix A. Supporting information

Supplementary data associated with this article can be found in the online version at http://dx.doi.org/10.1016/j.memsci.2018.01.021.

References

[1] W.J. Koros, C. Zhang, Materials for next-generation molecularly selective synthetic membranes, Nat. Mater. 16 (3) (2017) 289–297.
[2] M. Rungta, G.B. Wenz, C. Zhang, L. Xu, W. Qiu, J.S. Adams, W.J. Koros, Carbon molecular sieve structure development and membrane performance relationships, Carbon 115 (2017) 237–248.
[3] O. Sanyal, C. Zhang, G.B. Wenz, S. Fu, N. Bhuwania, L. Xu, M. Rungta, W.J. Koros, Next generation membranes – using tailored carbon, Carbon 127 (2018) 688–698.
[4] L. Xu, Carbon Molecular Sieve Hollow Fiber Membranes for Olefin/paraffin Separations (Ph.D. dissertation), Georgia Institute of Technology, 2012.
[5] N. Bhuwania, Y. Labreche, C.S.K. Achoundong, J. Baltazar, S.K. Burgess, S. Karwa, L. Xu, C.L. Henderson, P.J. Williams, W.J. Koros, Engineering substructure morphology of asymmetric carbon molecular sieve hollow fiber membranes, Carbon 76 (2014) 417–434.
[6] N. Bhuwania, Engineering the Morphology of Carbon Molecular Sieve (Cms) Hollow Fiber Membranes (Ph.D. dissertation), Georgia Institute of Technology, 2014.
[7] M. Kiyono, P.J. Williams, W.J. Koros, Effect of polymer precursors on carbon molecular sieve structure and separation performance properties, Carbon 48 (15) (2010) 4432–4441.
[8] D.T. Clausi, W.J. Koros, Formation of defect-free polyimide hollow fiber membranes for gas separations, J. Membr. Sci. 167 (1) (2000) 79–89.
[9] G.B. Wenz, W.J. Koros, Tuning carbon molecular sieves for natural gas separations: a diamine molecular approach, AIChE J. 63 (2) (2017) 751–760.
[10] C. Zhang, G.B. Wenz, P.J. Williams, J.M. Mayne, G. Liu, W.J. Koros, Purification of aggressive supercritical natural gas using carbon molecular sieve hollow fiber membranes, Ind. Eng. Chem. Res. 56 (37) (2017) 10482–10490.
[11] M.C. Douskey, M.S. Gebhard, A.V. McCormick, B.C. Lange, D.W. Whitman, M.R. Schure, K. Beshah, Spectroscopic studies of a novel cyclic oligomer with pendant alkoxysilane groups, Prog. Org. Coat. 45 (2) (2002) 145–157.
[12] D.Q. Vu, W.J. Koros, S.J. Miller, High pressure CO2/CH4 separation using carbon molecular sieve hollow fiber membranes, Ind. Eng. Chem. Res. 41 (3) (2002) 367–380.
[13] D. Pye, H. Hoehn, M. Panar, Measurement of gas permeability of polymers. I. Permeabilities in constant volume/variable pressure apparatus, J. Appl. Polym. Sci. 20 (7) (1976) 1921–1931.
[14] M.G. Kamath, S. Fu, A.K. Itta, W. Qiu, G. Liu, R. Swaidan, W.J. Koros, 6FDA-DETDA: DABE polyimide-derived carbon molecular sieve hollow fiber membranes: circumventing unusual aging phenomena, J. Membr. Sci. 546 (2018) 197–205.
[15] J. Adams, N. Bighane, W.J. Koros, Pore morphology and temperature dependence of gas transport properties of silica membranes derived from oxidative thermolysis of polydimethylsiloxane, J. Membr. Sci. 524 (2017) 585–595.
[16] K.-S. Liao, Y.-J. Fu, C.-C. Hu, J.-T. Chen, Y.-H. Huang, M. De Guzman, S.-H. Huang, K.-R. Lee, Y. Jean, J.-Y. Lai, Development of the asymmetric microstructure of carbon molecular sieve membranes as probed by positron annihilation spectroscopy, J. Phys. Chem. C 117 (7) (2013) 3556–3562.
[17] K.M. Steel, W.J. Koros, An investigation of the effects of pyrolysis parameters on gas separation properties of carbon materials, Carbon 43 (9) (2005) 1843–1856.
[18] M.S. McCaig, D.R. Paul, Effect of film thickness on the changes in gas permeability of a glassy polyarylate due to physical aging Part I. Experimental observations, Polymer 41 (2) (2000) 629–637.
[19] M.S. McCaig, D.R. Paul, J.W. Barlow, Effect of film thickness on the changes in gas permeability of a glassy polyarylate due to physical aging Part II. Mathematical model, Polymer 41 (2) (2000) 639–648.